Int. J. Electrochem. Sci., 16 **(2021)** Article ID: 210847, doi: 10.20964/2021.08.47

International Journal of
ELECTROCHEMICAL
SCIENCE
www.electrochemsci.org

Short Communication

Investigation of Crevice Corrosion Behavior of HRB355 Steel in 3.5% NaCl solution using Coupled multi-electrode arrays

Yangyang Guo

Shijiazhuang University of Applied Technology, Shijiazhuang, Hebei, China, 050081
E-mail: lunwen0002021@163.com

Received: 24 April 2021 / *Accepted:* 9 June 2021 / *Published:* 30 June 2021

During its lifetime, the cracks formed in concrete can accelerate the corrosion process of steel rebars, resulting in the decrease in the steel area and corresponding strength of steel bars which might lead to even a catastrophic fracture. There have been a few studies carried out on the formation mechanism of corrosion cracks in concrete structures and the corrosion behavior of metals under alternate drying-wetting conditions. In this paper, the formation of crevice corrosion in concrete structures and the corrosion behavior of metal under alternate drying-wetting conditions have been analyzed by using array electrode and wedge-crevice structure. The results showed that the crevice corrosion in concrete can take place in two stages. During 0-36 h, the crevice area and the exposed area were divided into apparent cathode area and anode area, during which the diffusion process of corrosive medium at the interface and the formation process of oxygen concentration difference battery primarily took place. Within 36-72 h, the corrosion cracks were formed, and the experimental system was corroded by the difference of oxygen concentrations in the battery. With the increase in drying-wetting time, the corrosion driving force and the corrosion current density of the metal increased as well as the total corrosion rate and the max pit depth increased, whereas the pitting rate decreased. As the distance from the crack increased, the total corrosion rate decreased and the corresponding pitting rate increased, while the corrosion morphology changed from total corrosion to pitting corrosion.

Keywords: Array electrode; Crevice corrosion; Concrete; Wetting-drying circle

1. INTRODUCTION

During the service life of concrete, it may expands, crack, spall off, and even disintegrate, forming corrosion cracks, which provide channels for various corrosive media to enter it, thereby further accelerating the concrete deterioration [1-3]. Theoretically, when the size of these cracks is between 0.025 and 0.1 mm, the corrosive medium is easy to stay forming a sensitive area for crevice corrosion, which may cause crevice corrosion [4-7]. In addition, the crevice corrosion also has a strong concealment, and it may cause a certain degree of damage before it is revealed. This may result in a significant strength reduction of the steel rebars in concrete [8,9]. So far, various researchers have put

forward various studies focusing on the corrosion of block theory, composition change theory, the IR drop, low pH value, etc. However, the research findings on crevice corrosion of concrete rebar under alternate wetting and drying environment are relatively fewer [10-12]. Therefore, it is of great significance for understanding the formation process of crevice corrosion in concrete and revealing the characteristics of crevice corrosion under alternate drying-wetting environment, which will provide guideline for the optimization, improvement, and protection of concrete.

2. EXPERIMENT SETTINGS

HRB335 steel was used as the metal (rebar material) for the test. The main components are shown in Tab.1. The samples were cleaned with acetone, deionized water, anhydrous ethanol, and then dried and sealed for preservation. The analytically pure NaCl and deionized water were used as the experimental solution. The mass fraction of NaCl was 3.5%. The experimental devices were placed at a constant temperature in a humidity chamber. The experimental temperature was set at 25 ℃.

Table 1. Main components of HRB335 steel (wt.%)

Element	C	Si	Mn	P	S	Ceq
Content	0.25	0.80	1.60	0.045	0.045	0.52

2.1 Experimental tests based on array electrodes

Using plexi-glass plate as fixed plate, a 10×10 array of round holes was machined with a fine engraving machine. The aperture was 2 mm, and the spacing between the holes was 0.5 mm. The polished HRB335 steel wires with the diameter of 2 mm were inserted into the hole. The array electrodes were encapsulated with epoxy resin to ensure a complete barrier and insulation between the wires. After curing at room temperature for 72 h, the electrode array was polished so that it was completely leaked out of the metal matrix. Finally, the electrode was polished by metallographic abrasive paper until it was smooth, so as to reduce the experimental error caused by varying surface roughness. The treated electrode array was placed in a vacuum drying in the oven, for later use.

Half of the array electrode was covered by a transparent PE plate to form a rectangular gap system with a gap width of 0.1 mm, as shown in Fig.1(a). The experimental device was placed in NaCl solution, and the experiment period was set to 72 h. The LabVIEW program was designed to automatically collect the potential and current density of the array electrode with varying experimental time. The electrochemical impedance measurement range was 10^{2}–10^{-5} Hz, and the disturbance voltage was ±10 mV. Electrochemical data processing was performed using "ZSimpWin" software.

2.2 Experimental tests based on wedge crevice

The crevice corrosion environment of concrete was simulated by a wedge crevice experimental device, as shown in Fig.1(b). The upper and lower cover plates were made of PE material, and the gap

was set as 0.1 mm [13-15]. Six specimens with the area of 10×10 mm^2 were set at a distance of 0-15 cm from the crack. According to the electrochemical test method, the reference electrode (SCE) and the auxiliary electrode (Pt) were set up for every specimen, respectively, to test the change of corrosion kinetic parameters with time of 3-72 h. Princeton PARSTAT 2273 was used as the electrochemical workstation to obtain the corrosion potential (E_{corr}) and corrosion current density (I_{corr}).

In the experiment, the solution was filled with the wedge-crevice device followed by the draining of the corrosive medium to simulate the corrosion crack in concrete, in which the ratio of wetting and drying was set as 12h:12h. The experiment of alternate drying-wetting cycle was carried out for a period of 24 h with a total of 480 h (20 cycles). The samples were taken at different durations of 24 h, 72 h, 144 h, 288 h and 480 h, respectively. After the specimens were removed and cleaned, the overall corrosion rate was calculated (Eq.1) [16], while the surface morphology was observed by Zeiss Microscope to capture the 3D image features of HRB355 steel and then obtain the max pit depth to calculate pit corrosion rate (Eq.2) [17].

$$v_1 = 87600 \times \frac{\Delta G}{S \times t \times \rho} \tag{1}$$

Where, v_1 was total corrosion rate in mm/a, $\triangle G$ was the weight loss of HRB355 steel in g, S was surface area of 1 cm^2, t was experimental time in h and ρ was HRB355 density of 7.85 g/cm^3.

$$v_2 = 87600 \times \frac{H_{max}}{t} \tag{2}$$

Where, v_2 was pit corrosion rate in mm/a, H_{max} was the max pit depth obtained by Zeiss Microscope in mm and t was experimental time in h.

All experiments were carried out in constant temperature-humidity chamber "GDJS-408" at temperature 25 ℃.

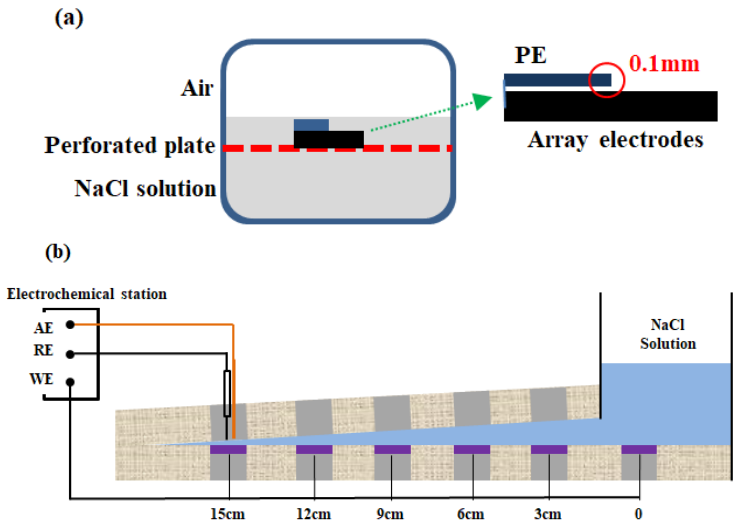

Figure 1. Experiment devices. (a) Experimental test based on array electrode, (b) Experimental test based on wedge crevice

3. RESULTS AND DISCUSSION

3.1 Electrochemical characteristics of corrosion crevice formation

Fig.2 shows the variation of potential and current density distribution on the surface of HRB355 steel array electrodes with time of 3-72 h in 3.5 wt.% NaCl solution at temperature 25 ℃. Fig.3 shows the difference of electrode potential and current density between the crevice area and the exposed area of HRB355 steel array electrodes with time of 3-72 h in 3.5 wt.% NaCl solution at temperature 25 ℃.

With the corrosive medium diffusing into the crevice area, it could be seen that in 3 h, the metal potential in the exposed area was apparently negative to the metal potential in the crevice area. The potential in the crevice area gradually declined and was more negative, changing from the cathode area to the anode area at the initial moment. When the experiment lasted for 12 h, the metal potential in the exposed area continued to shift negatively [18-20].

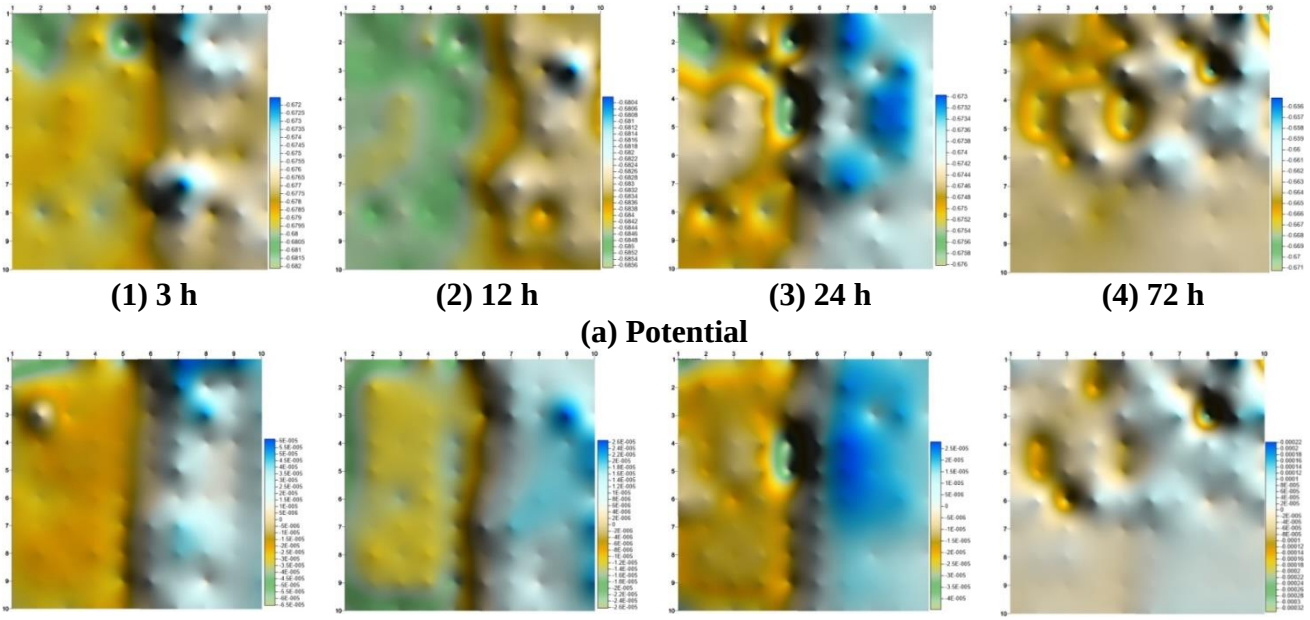

(1) 3 h **(2) 12 h** **(3) 24 h** **(4) 72 h**

(a) Potential

(1) 3 h **(2) 12 h** **(3) 24 h** **(4) 72 h**

(b) Current density

Figure 2. The variation of surface potential and current density distribution of HRB355 steel array electrodes with time of 3-72 h in 3.5 wt.% NaCl solution at temperature 25 ℃

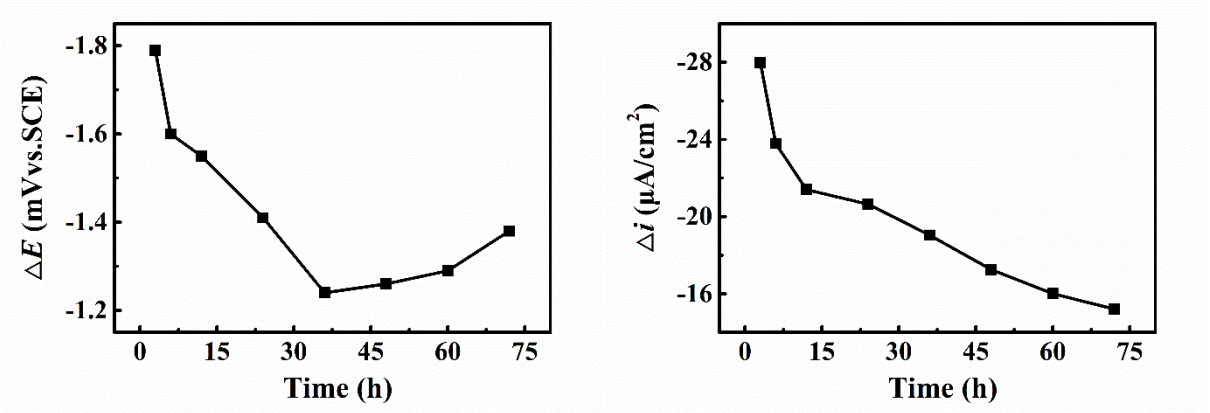

Figure 3. Difference of potential and current density between crevice area and exposed area of HRB355 steel array electrodes with time of 3-72 h in 3.5 wt.% NaCl solution at temperature 25 ℃

Meanwhile, due to the diffusion of corrosive media at the interface, the anode area of the whole system increased. In the following 12 h, it can be seen from the surface potential distribution image that the overall difference of potential decreased. Due to the closed structure of the crevice, the oxygen concentration difference battery was formed in the whole area, thus, intensifying the corrosion. The beginning of forming the oxygen concentration cell at 36 h can also be seen from the Fig.3. Further, the potential difference of crevice area and exposed area continuously decreased, and then slightly increased. It can be seen from the potential distribution at 72 h that the typical crevice corrosion had been formed at this time. In terms of the surface distribution of current density, the entire current distribution was divided into two distinct regions by crevice area and exposed area within 0-36 h. When the experiment was carried out for 72 h, the current density in the local area decreased significantly. As can be seen from the current difference curve in Fig.3, with the progress of the experiment, the current difference gradually decreased indicating that the corrosion cracks were formed in the whole area and the autocatalytic process was the main phenomenon in the cracks. Fig.4 shows the characteristic EIS curves of HRB355 steel with time of 1-72 h in 3.5 wt.% NaCl solution at temperature 25 ℃. Tab.2 shows the fitting results of Nyquist diagrams of HRB355 steel with time of 1-72 h in 3.5 wt.% NaCl solution at temperature 25 ℃. In the whole experiment, according to the fitting circuit and the test results, the reaction process (1-72 h) can be divided into two stages.

The first stage lasted from 1-24 h. As can be seen from Fig.4, with the experiment being carried out, the EIS curves showed that the capacitive reactance arc was connected to the diffusion impedance at 1 h. So the equivalent circuit was chosen as $R_s(Q(R_pW(C_{dl}R_{ct})))$; where '$R_s$', 'Q', '$R_p$', '*W'*, '$C_{dl}$', and '$R_{ct}$' are the solution resistance, system capacitance, polarization resistance, Weber diffusion impedance, double-layer capacitance, and the charge transfer resistance, respectively. This indicates that the electrolyte had gradually diffused at the interface. In the neutral solution, the oxygen absorption reactions mainly occurred at the cathode ($O_2+2H_2O+4e^-\rightarrow 4OH^-$) and at the anode ($Fe\rightarrow Fe^{2+}+2e^-$) [21]. When the experiment continued for 12 h, the whole process was still dominated by the diffusion without obvious crevice corrosion characteristics. At this time, the system capacitance '*Q*' increased, the resistance 'R_p' decreased, and the diffusion impedance could be defined as "not ideal" (Weber impedance $n\approx 0.75$). When the experiment continued till 24 h, the diffusion impedance

tail still existed, but the capacitive reactance arc diameter decreased significantly. At this time, both *'Q'* and 'R_p' increased significantly, indicating that the oxygen concentration difference battery was progressively formed.

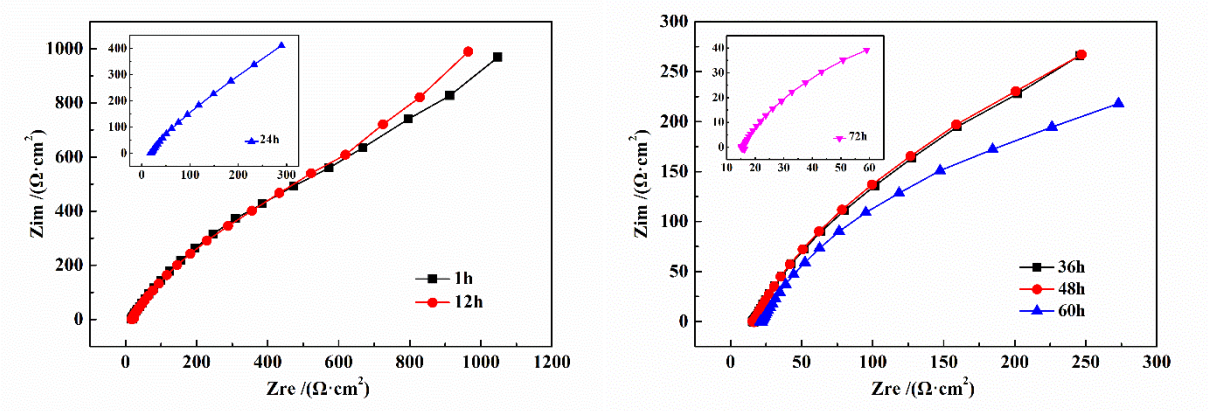

Figure 4. Nyquist diagrams of HRB355 steel with time of 1-72 h in 3.5 wt.% NaCl solution at temperature 25 ℃

The second stage lasted for 36-72 h. When the experiment was carried out for 36 h, the diffusion impedance had disappeared and the EIS curves showed a capacitive reactance feature. At this time, it entered the second stage, so the equivalent circuit $R_s(Q(R_p(C_{dl}R_{ct})))$ was selected. With the progress of the reaction, the oxygen concentration cell was formed. At this time, only the dissolution and hydrolysis of metal occurred in the crevice ($Fe+2H_2O \rightarrow Fe(OH)_2+2H^+ + 2e^-$). In the subsequent time, the corrosion mechanism of the whole system was mainly due to the oxygen concentration difference.

Table 2. Fitted results of equivalent electric circuits of Nyquist diagrams of HRB355 steel with time of 1-72 h in 3.5 wt.% NaCl solution at temperature 25 ℃

Parameter \ Time	1 h	12 h	24 h	36 h	48 h	60 h	72 h
R_s (Ω·cm²)	5.36	5.54	5.85	4.98	5.01	6.77	4.90
Q (F/cm²)	6.70×10^{-3}	7.33×10^{-3}	4.17×10^{-2}	4.59×10^{-2}	4.65×10^{-3}	4.40×10^{-3}	1.77×10^{-1}
n	0.75	0.76	0.77	0.70	0.71	0.71	0.55
R_p (Ω·cm²)	299.50	236.04	243.92	2.23	2.67	4.19	0.49
Z_w (Ω·cm²)	8.81×10^{-3}	8.03×10^{-3}	1.62×10^{-2}	-	-	-	-
C_{dl} (F/cm²)	-	-	-	8.31×10^{-3}	8.53×10^{-3}	8.68×10^{-3}	1.20×10^{-1}
R_{ct} (Ω·cm²)	-	-	-	342.82	334.66	217.74	59.19

Fig.5 shows the variation of Bode plots of HRB355 steel with time of 1-72 h in 3.5 wt.% NaCl solution at temperature 25 ℃. Based on the phase angle and impedance, the whole experimental process can be divided into two stages. In the first stage (0-24 h), when the frequency f=0.5 Hz, the

maximum phase angle, namely the "peak" value, was about 55°. At this time, the diffusion of corrosive media to the interface of the crevice region took place. When the experiment was further proceeded to the second stage, the maximum phase angle at the test point at 36 h slightly increased compared to the value at 24 h. It can be seen from Fig.4 that the system capacitance increased significantly at 36 h while the corrosion crevice and double electric layer were gradually formed. With the further increase in experimental time, the maximum phase angle appeared at the frequency f=0.07Hz and then gradually dropped This showed that the oxygen concentration difference in the corrosion process was dominant in this stage [22,23].

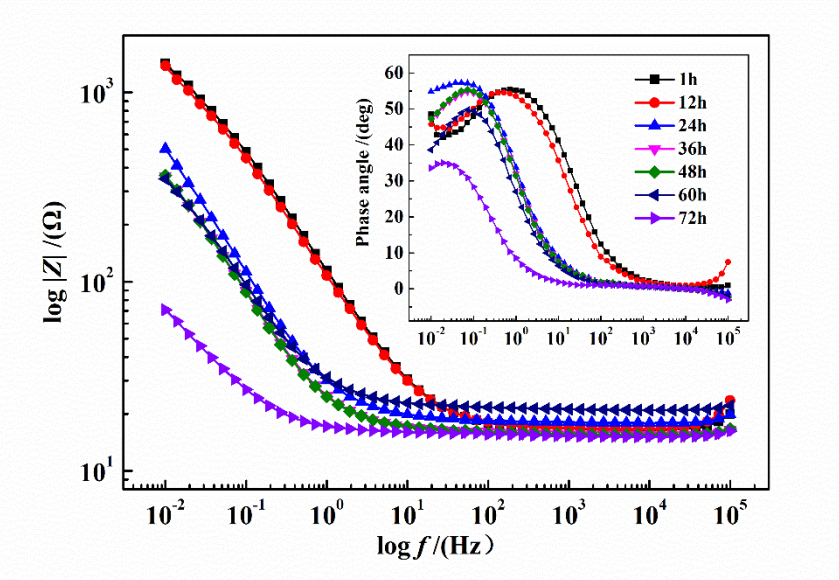

Figure 5. Bode plots of HRB355 steel with time of 1-72 h in 3.5 wt.% NaCl solution at temperature 25 ℃

3.2 Corrosion behavior of metal under wetting-drying conditions

Fig.6 and Fig.7 show the change curves of the overall corrosion rate, max pit depth, and pit corrosion rate of the metal, at different distances from the crack of 0-15 cm, with experimental time of 24-480 h, whereas Fig.8 shows the 3D image features of HRB355 steel at different distances from the crack of 0-15cm at 480 h in 3.5 wt.% NaCl solution at temperature 25 ℃.

As can be seen from the Fig.6, the overall corrosion rate of the metal at different distances increased rapidly with experimental time. Meanwhile, with the increase in gap distance, the total corrosion rate decreased at different times. Under the experimental conditions of this paper, the total corrosion rate of the metal with a distance of 0 cm was 0.56 mm/a at 24 h, while that of the metal with a distance of 15 cm was 0.41 mm/a. However, at 480 h these increased to 1.55 mm/a and 1.00 mm/a, respectively, which further increased by 2.77 and 2.44 times, indicating the oxygen was the key parameter for the crevice corrosion under alternate wetting-drying conditions [24-26].

For the pit characteristics, with the increase in experimental time the max pit depth increased, whereas the pit corrosion rate gradually decreased, and ultimately stayed constant. Moreover, under

the same time condition, the greater the distance from the crack was, the greater was the maximum pit depth [27].

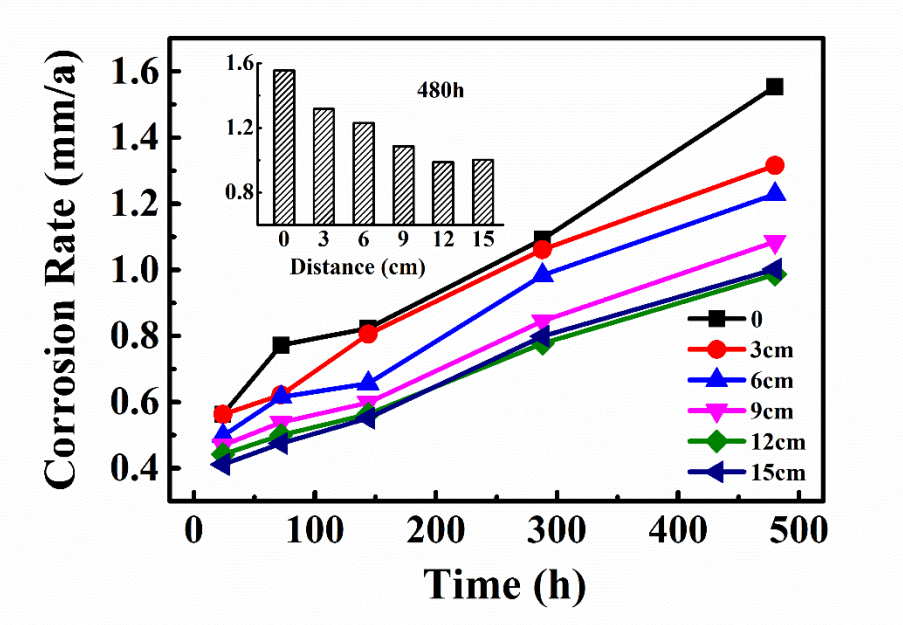

Figure 6. The change curves of the overall corrosion rate of the HRB355 steel at different distances from the crack of 0-15cm with experimental time of 24-480 h in 3.5 wt.% NaCl solution at temperature 25 ℃

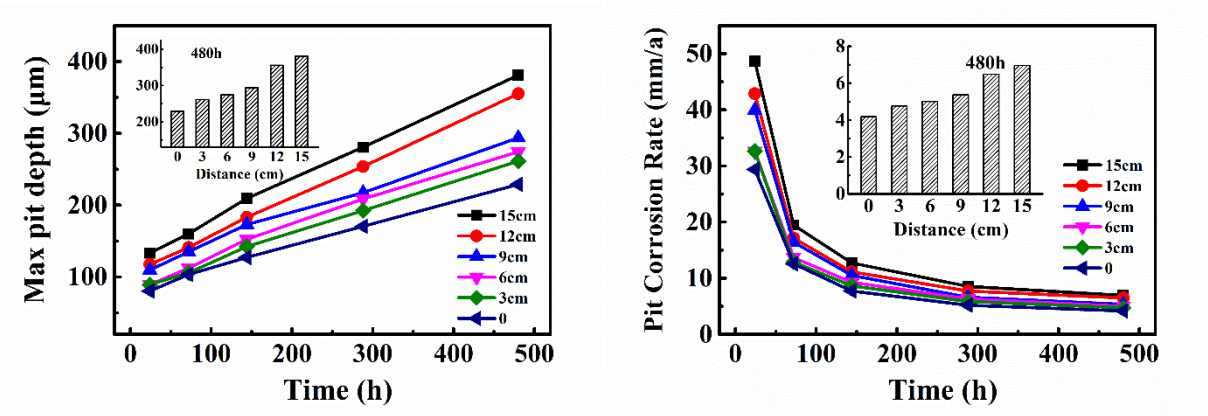

Figure 7. The change curves of the max pit depth and pit corrosion rate of the HRB355 steel at different distances from the crack of 0-15cm with experimental time of 24-480 h in 3.5 wt.% NaCl solution at temperature 25 ℃

According to the 3D scanning image of the max pit depth measured in Fig. 8, when the distance increased from 0 to 3 cm at 480 h, the unevenness of the sample surface increased. However, there was no obvious pit corrosion on the whole surface. The overall corrosion process was the main activity taking place. When the distance increased to 6 cm and 9 cm, the local typical pitting features appeared on the sample surface, but the pitting aperture was large. With the further increase in the distance, the

pitting features were typical when the distance was 12 cm [28,29]. Furthermore, the larger the distance was, the smaller the pit aperture and the greater the depth were, as shown in the Fig.8 (when the distance was 15 cm).

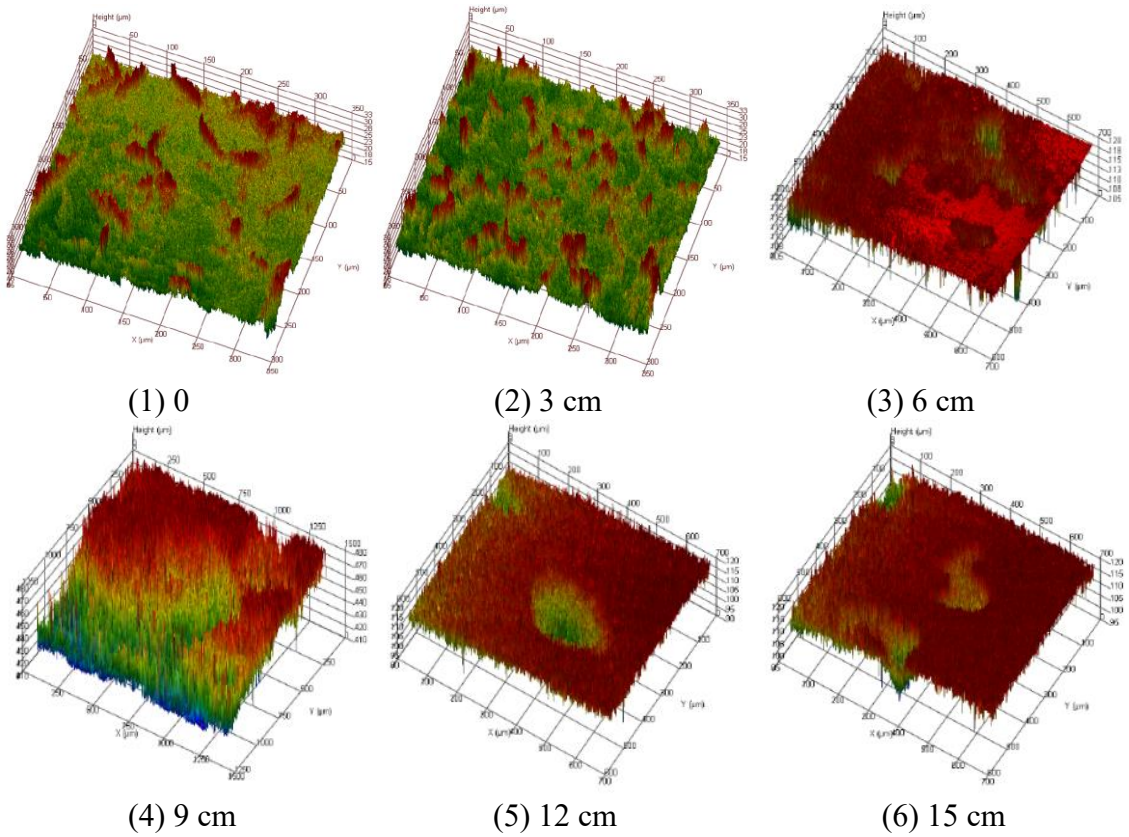

(1) 0 (2) 3 cm (3) 6 cm

(4) 9 cm (5) 12 cm (6) 15 cm

Figure 8. The 3D image features of HRB355 steel at different distances from the crack of 0-15cm at 480 h in 3.5 wt.% NaCl solution at temperature 25 ℃

3.3 E_{corr} and I_{corr} of metal under wetting-drying conditions

Fig. 9 shows the change curves of corrosion potential (E_{corr}) and corrosion current density (I_{corr}) of HRB355 steel at different distances from the crack of 0-15cm with experimental time of 0-480 h in 3.5 wt.% NaCl solution. For corrosion current density, "+" was the cathode current density and "-" was the anode current density.

It can be seen that with the increase in experimental time, the 'E_{corr}' of metal at different distances shifted to a negative direction. The greater the distance was, the greater the degree of negative deviation was identified, indicating that the greater the gap depth was, the greater was the metal corrosion tendency. For the whole experimental device, as mentioned earlier, the oxygen concentration battery was formed with anode inside the crevice and cathode outside the crevice. From the 'E_{corr}' of metals with a distance of 0 and 15 cm, with the increase in experimental time the potential

difference of oxygen concentration battery increased, meaning that the corrosion driving force and the tendency to accelerate the corrosion increase. According to the test results of 'I_{corr}', at the initial stage, the 'I_{corr}' of the samples at different positions remained unchanged, while as the experiment progressed both the cathode current density and the anode current density of the system showed an increasing trend [30].

Thus, the potential difference of the system increased with time providing a much stronger corrosion driving force, while the increase in 'I_{corr}' indicated that the corrosion in the crevice intensified, which may be attributed to the development of pitting corrosion.

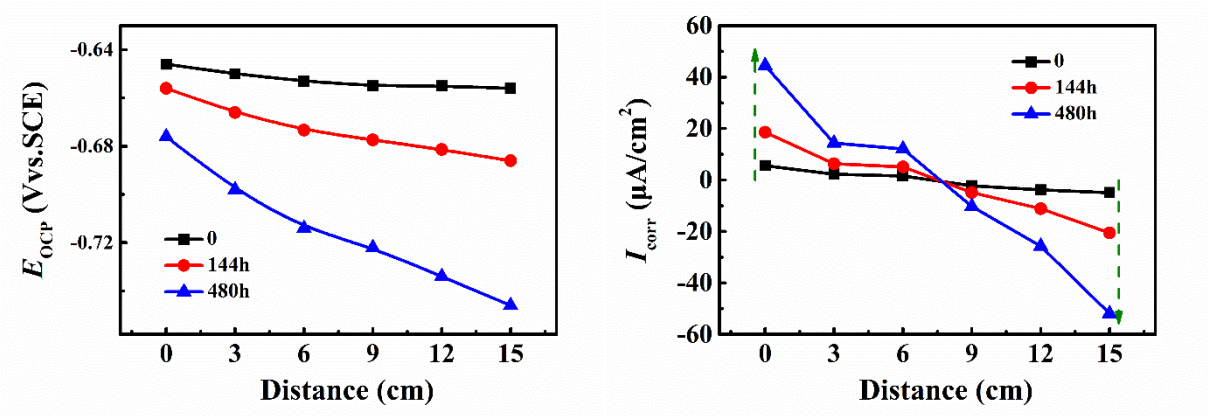

Figure 9. Change curves of corrosion potential (E_{corr}) and corrosion current density (I_{corr}) of HRB355 steel at different distances from the crack of 0-15cm with experimental time of 0-480 h in 3.5 wt.% NaCl solution at temperature 25 ℃

4. CONCLUSION

Based on the array electrode and the wedge-crevice device, the formation mechanism of crevice corrosion structure of concrete and the corrosion behavior of metal under alternate wetting-drying cycles have been analyzed in this paper. The main conclusions were as under:

(1) With the diffusion of corrosive media into the crevice, the crevice area and the exposed area were divided into cathode area and anode area within 0-36 h. However, the potential difference gradually decreased. The EIS characteristics were shown as Weber impedance diffusion, which represented the diffusion process of corrosive media at the interface and the formation of oxygen concentration difference battery. Within 36-72 h, the corrosion cracks were formed, and the experimental system was primarily corroded by oxygen concentration difference battery.

(2) With the increase in the drying-wetting time, the corrosion driving force and the corrosion current density of the metal increased. The overall corrosion rate and the max pit depth of the metal increased, whereas the pitting rate decreased. As the distance from the crack increased, the total corrosion rate decreased and the pitting rate increased, whereas the corrosion morphology changed from the total corrosion to the pitting corrosion.

References

1. R.D. Moser, P.M. Singh, L.F. Kahn, K.E. Kurtis, D.G. Nino and Z.B. Mcclelland, *Constr. Build. Mater.*, 203 (2019) 366.
2. B. Saassouh and Z. Lounis, *Cement Concrete Comp.*, 34 (2012) 1082.
3. T. Mori, M. Koga, Y. Hikosaka, T. Nonaka, F. Mishina, Y Sakai and J. Koizumi, *Water Sci. Technol.*, 23 (2011) 1275.
4. T. Fatima, N. Arab, E.P. Zemskov and A. Muntean, *J. Eng. Math.*, 69 (2010) 261.
5. G. Jiang, J. Keller, P.L. Bond and Z. Yuan, *Water Res.*, 92 (2016) 52.
6. C. Jiang, Y.F. Wu and M.J. Dai, *Constr. Build. Mater.*, 158 (2018) 1073.
7. Y.S. Ji , G. Zhan, Z. Tan, Y. Hu and F. Gao, *Constr. Build. Mater.*, 79 (2015) 214.
8. C. Yang, Q Han, A Wang, Y Yang and X Li, *AIP Adv.*, 11 (2021) 035217.
9. D. Neff, J. Harnisch, M. Beck, V. L'Hostis, J. Goebbels and D. Meinel, *Mater. Corros.*, 62 (2015) 861.
10. J. Wei, X.X. Fu, J.H. Dong and W. Ke, *J. Mater. Sci. Technol.*, 10 (2012) 43.
11. U. Angst, *Electrochim. Acta*, 56 (2011) 5877.
12. G. Jiang, M. Zhou, T.H. Chiu, X. Sun, J. Keller and P.L. Bond, *Environ. Sci. Technol.*, 50 (2016) 8084.
13. Y. Zhao, Y. Jiang, B. Hu and W Jin, *Corros. Sci.*, 55 (2012) 385.
14. A. Thybo, A. Michel and H. Stang, *Mater. Struct.*, 50 (2018) 146.
15. G. Jiang, X. Sun, J. Keller and P.L. Bond, *Water Res.*, 80 (2015) 30.
16. S. Hong, H. Wiggenhauser, R. Helmerich, B. Dong, P. Dong and F. Xing, *Corros. Sci.*, 114 (2016) 123.
17. J. Blunt, G. Jen and C.P. Ostertag, *Corros. Sci.*, 92 (2015) 182.
18. S. Soleimani, P. Ghods, O.B. Isgor and J. Zhang, *Cement Concrete Comp.*, 32 (2010) 360.
19. C. Chong, M. Cheung and B. Chan B, *Corros. Sci.*, 69 (2013) 97.
20. M. Nehdi, M.S. Alam and M.A. Youssef, *Eng. Struct.*, 32 (2010) 2518.
21. N.D. Stambaugh, T.L. Bergman and W.V. Srubar, *Constr. Build. Mater.*, 161 (2018) 236.
22. M.G. Sohail, R. Kahraman, N.A. Alnuaimi, B. Gencturk and A. Belarbi, *Constr. Build. Mater.*, 232 (2020) 117205.
23. O.B. Isgor and A.G. Razaqpur, *Mater. Struct.,* 39 (2006) 291.
24. T. Wang, K. Wu, L. Kan and M. Wu, *Constr. Build. Mater.*, 247 (2020) 118539.
25. Y. Xie, X. Lin, W. Pan, T. Ji, Y.N. Liang and H. Zhang, *Constr. Build. Mater.*, 188 (2018) 9.
26. Y. Zhao, J. Dong, Y. Wu and W. Jin, *Constr. Build. Mater.*, 116 (2016) 273.
27. S. Muthulingam and B.N. Rao, *Corros. Sci.*, 93 (2015) 267.
28. C. Grengg, F. Mittermayr, A. Baldermann, M.E. Ttcher, A. Leis, G. Koraimann, P. Grunert and M. Dietzel, *Cement Concrete Res.*, 77 (2015) 16.
29. V. Shubina, L. Gaillet, T. Chaussadent, T. Meylheuc and J. Creus, *J. Clean. Prod.*, 112 (2016) 666.
30. P. Zhang, Y. Cong, M. Vogel, Z. Liu, H.S. Mueller, Y. Zhu and T. Zhao, *Constr. Build. Mater.*, 148 (2017) 113.